

## Electromagnetohydrodynamic response of a plasma to an external current pulse

H. B. Zhou, K. Papadopoulos, A. S. Sharma, and C. L. Chang

Citation: *Physics of Plasmas* (1994-present) **3**, 1484 (1996); doi: 10.1063/1.872009

View online: <http://dx.doi.org/10.1063/1.872009>

View Table of Contents: <http://scitation.aip.org/content/aip/journal/pop/3/5?ver=pdfcov>

Published by the [AIP Publishing](#)

---

### Articles you may be interested in

Erratum: "Pulsed currents carried by whistlers. VI. Nonlinear effects; VII. Helicity and transport in heat pulses" [*Phys. Plasmas* **3**, 2589 and 2599 (1996)]

*Phys. Plasmas* **4**, 249 (1997); 10.1063/1.872616

[Pulsed currents carried by whistlers. VI. Nonlinear effects](#)

*Phys. Plasmas* **3**, 2589 (1996); 10.1063/1.872080

[Pulsed currents carried by whistlers. VII. Helicity and transport in heat pulses](#)

*Phys. Plasmas* **3**, 2599 (1996); 10.1063/1.872079


[Pulsed currents carried by whistlers. IV. Electric fields and radiation excited by an electrode](#)

*Phys. Plasmas* **2**, 1114 (1995); 10.1063/1.871390

[Pulsed currents carried by whistlers. III. Magnetic fields and currents excited by an electrode](#)


*Phys. Plasmas* **2**, 1100 (1995); 10.1063/1.871389

---

A collection of five pieces of Pfeiffer Vacuum equipment, including a red turbopump, a silver turbopump, a white turbopump, a red turbopump with a long shaft, and a silver chamber component.

 Vacuum Solutions from a Single Source

- Turbopumps
- Backing pumps
- Leak detectors
- Measurement and analysis equipment
- Chambers and components

**PFEIFFER**  VACUUM

# Electromagnetohydrodynamic response of a plasma to an external current pulse

H. B. Zhou,<sup>a)</sup> K. Papadopoulos, and A. S. Sharma  
*University of Maryland, College Park, Maryland 20742*

C. L. Chang  
*Science Applications International Corp., McLean, Virginia 22101*

(Received 30 June 1995; accepted 1 February 1996)

In this paper we examine the dynamic response of a magnetoplasma to an external time-dependent current source in the context of electronmagnetohydrodynamics (EMHD). A combined analytic and numerical technique is developed to address this problem. The set of cold electron plasma and Maxwell's equations are first solved analytically in the  $(\mathbf{k}, \omega)$  space. Inverse Laplace and three-dimensional complex Fast Fourier Transform techniques are used subsequently to numerically transform the radiation fields and plasma currents from the  $(\mathbf{k}, \omega)$  space to the  $(\mathbf{r}, t)$  space. The results show that the electron plasma responds to a time-varying current source imposed across the magnetic field by exciting whistler/helicon waves and forming an expanding local current loop, driven by field-aligned plasma currents. The current loop consists of two antiparallel field-aligned current channels concentrated at the ends of the imposed current and a cross-field Hall current region connecting these channels. The characteristics of the current closure region are determined by the background plasma density, the magnetic field, and the time scale of the current source. The results are applied to the ionospheric generation of extremely low-frequency (ELF) and very low-frequency (VLF) radiation using amplitude modulated high-frequency heating. It is found that contrary to previous suggestions the dominant radiating moment of the ELF/VLF ionospheric source is an equivalent horizontal magnetic dipole. © 1996 American Institute of Physics. [S1070-664X(96)01805-4]

## I. INTRODUCTION

The transient response of a magnetoplasma to externally imposed stationary or moving current pulses is a fundamental plasma physics problem with a wide range of applications. The formal solution of this problem for a cold, collisionless, isotropic plasma is well known.<sup>1</sup> Kuehl<sup>2</sup> used the far-zone dyadic Green's function to calculate the radiation of an electric dipole in a two-dimensional (2-D) magnetoplasma. A solution was found only for the case when the frequency  $\omega$  is much higher than the electron plasma frequency  $\omega_e$  and the electron cyclotron frequency  $\Omega_e$ , viz.  $\omega/\omega_e \gg 1$  and  $\omega/\Omega_e \gg 1$ . For low frequencies,  $\omega < \Omega_e$ , the integral equation reduces to a transcendental equation that cannot be solved analytically. Vidmar<sup>3</sup> used a saddle point method to study the delta function excitation of waves in the Earth's ionosphere in one dimension. He found an asymptotic solution, valid for the far-zone field and long after the source turn-on. Transient effects were lost through the use of the saddle point method. Furthermore, saddle point methods are very difficult to use<sup>4</sup> for multidimensional cases. Because of the mathematical difficulty in calculating the integrals analytically in two or three dimensions, numerical solutions are required.

The objective of this paper is to study the transient re-

sponse of a magnetoplasma to a current pulse, in the parameter range where the ratio of the electron cyclotron to electron neutral collision frequency ( $\nu_e$ ) is larger than unity, while the ratio of the ion cyclotron to the ion neutral collision frequency ( $\nu_i$ ) is smaller than unity. This is the case for the plasma in the D and E regions of the ionosphere between 70–130 km altitude range. At high latitudes this region is penetrated by electric fields and currents. As a result, transient precipitation events that cause local conductivity modifications induce current pulses, to which the plasma responds by generating electromagnetic (EM) waves and currents. Of particular interest is the plasma response to periodic heating of the D region by ionospheric high-frequency (HF) radio wave heaters. This phenomenon is extremely important, since it leads to the generation of low-frequency EM waves in the ultra low-frequency (ULF), extremely low-frequency (ULF), and very low-frequency (VLF) ranges.<sup>5–8</sup> A new technique that combines analytic and numerical methods is developed in this paper. The electron plasma and Maxwell's equations are solved analytically in Fourier space; then inverse complex fast Fourier transform (FFT) technique is used to transform the radiation fields and plasma currents from Fourier space into real space and time. A general form of time-varying current source is used, and collisional effects on the plasma response are retained. This paper is organized as follows. In the next section we discuss the dielectric properties of the D region and present the model used in the

<sup>a)</sup>Current address: GE Capital Spacenet Services, Inc., 1750 Old Meadow Road, McLean, Virginia 22102-4300.

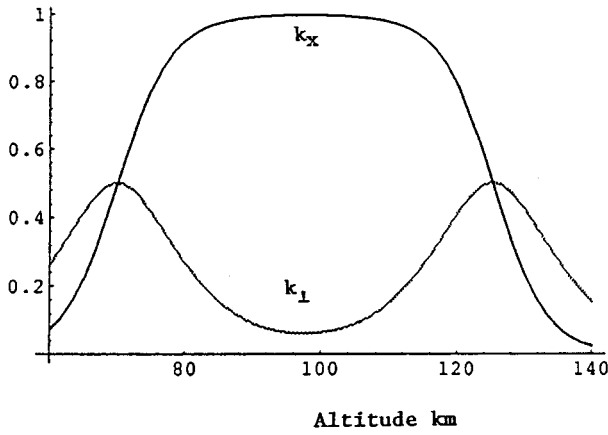


FIG. 1.  $K_{\perp}(z)$  and  $K_x(z)$  as functions of altitude for typical ionospheric parameters.

computations. In Sec. III we present the basic set of equations and the methods used to obtain their solutions. The computational results are discussed in Sec. IV. In Sec. V we discuss the application of the model to the generation of ELF/VLF waves in ionospheric heating. In the final section we summarize the results and present suggestions for future studies.

## II. EIGENMODES OF THE LOWER IONOSPHERE

The linear wave equation describing electromagnetic wave propagation excited by a current  $\mathbf{J}_s(\mathbf{r}, t)$  in a vertically stratified ionosphere is given by<sup>9</sup>

$$-\nabla \times (\nabla \times \mathbf{E}) + \frac{\omega_e^2(z)}{c^2} \frac{1}{\Omega_e} \mathbf{G}(z) \cdot \frac{\partial \mathbf{E}}{\partial t} = \frac{4\pi}{c^2} \frac{\partial \mathbf{J}_s(z, t)}{\partial t}, \quad (1)$$

where

$$\mathbf{G}(z) = \begin{bmatrix} K_{\perp}(z) & K_x(z) & 0 \\ -K_x(z) & K_{\perp}(z) & 0 \\ 0 & 0 & K_z(z) \end{bmatrix}, \quad (2)$$

$$K_{\perp} = \frac{\epsilon}{1 + \epsilon^2}, \quad K_x = \frac{1}{1 + \epsilon^2}, \quad K_z = \frac{\Omega_e}{\nu_e}, \quad (3)$$

and

$$\epsilon = \frac{\nu_e}{\Omega_e} + \frac{\Omega_i}{\nu_i}. \quad (4)$$

In deriving Eqs. (1)–(4) a vertical magnetic field  $\mathbf{B} = \hat{z}B_0$  was assumed and  $\nu_e(\nu_i)$  is the electron (ion) neutral collision frequency. Figure 1 shows plots of  $K_{\perp}(z)$  and  $K_x(z)$  as a function of altitude for typical ionospheric parameters. The important aspect of Fig. 1 is that for  $z > 130$  km the diagonal elements of  $\mathbf{G}(z)$  dominate, giving rise to the traditional low-frequency Alfvén waves. However, for  $70 \text{ km} < z < 130$  km, the off-diagonal elements dominate, even for frequencies approaching zero. Since the value of  $\epsilon \ll 1$ , only the electron dynamics is important and the magnetized plasma modes resemble the well-known helicon modes in solid state plasmas.<sup>10,11</sup> The importance of this mode for the lower ionosphere can be seen by referring to the dispersion relation of the plasma in the 70–130 km altitude range for parallel propagation ( $k = \hat{z}k$ ). This is given by

sphere can be seen by referring to the dispersion relation of the plasma in the 70–130 km altitude range for parallel propagation ( $k = \hat{z}k$ ). This is given by

$$\left(\frac{kc}{\omega}\right)^2 = 1 - \frac{\omega_e^2}{\omega(\omega - i\nu_e - \Omega_e)} - \frac{\omega_i^2}{\omega(\omega - i\nu_i - \Omega_i)}. \quad (5)$$

For  $\omega < \Omega_i < \nu_i$ ,  $\nu_e \ll \Omega_e$ , and neglecting the displacement current, we obtain

$$\omega = k^2 c^2 \frac{\Omega_e}{\omega_e^2} \left[ 1 - i \left( \frac{\nu_e}{\Omega_e} + \frac{\Omega_i}{\nu_i} \right) \right]. \quad (6)$$

This is the helicon mode and suffers weak attenuation, even for  $\omega \ll \nu_e, \nu_i$ . The important aspect of the above analysis is that in the 70–130 km range the plasma response is controlled by electron dynamics, not only in the usual whistler range ( $\Omega_i < \omega < \Omega_e$ ), but also in the low-frequency range ( $\omega < \Omega_i$ ). As a result, when the plasma response to externally induced perturbations is considered, it is sufficient to retain only the electron dynamics and ignore the motion of the ions. Such a model is referred to as the electronmagnetohydrodynamic (EMHD) model and is described in the next section.

## III. IONOSPHERIC PLASMA MODEL

We study below the response of an electron plasma to a time-dependent and bounded current source  $\mathbf{J}_s(\mathbf{r}, t)$ . The plasma is modeled by the EMHD equations, which, as discussed in Sec. II, are the equations that describe the plasma in the range between 70–130 km in the ionosphere. Assuming a homogeneous, cold plasma with the ions forming a stationary neutralizing background, the EMHD equations are<sup>12</sup>

$$\nabla \times \mathbf{B} = -\frac{4\pi}{c} en_0 \mathbf{V}_e + \frac{4\pi}{c} \mathbf{J}_s, \quad (7)$$

$$\frac{d\mathbf{V}_e}{dt} = -\frac{e}{m_e} \left( \mathbf{E} + \frac{1}{c} \mathbf{V}_e \times \mathbf{B}_0 \right) - \nu_e \mathbf{V}_e, \quad (8)$$

$$\nabla \times \mathbf{E} = -\frac{1}{c} \frac{\partial \mathbf{B}}{\partial t}, \quad (9)$$

where  $n_0$  is the electron density,  $\mathbf{V}_e$  is the electron fluid velocity,  $\mathbf{E}$  and  $\mathbf{B}$  are the radiation fields, and  $\mathbf{J}_s$  is the externally driven current source, whose form will be specified later. The dominant plasma response enters through the first term on the right-hand side of Eq. (7). The displacement current has been neglected since we are interested only in low frequencies. From Eqs. (7)–(9) we obtain for the evolution of the magnetic field  $\mathbf{B}(\mathbf{r}, t)$ ,

$$\begin{aligned} \frac{\partial}{\partial t} \nabla^2 \mathbf{B} + \nu_e \nabla^2 \mathbf{B} - \frac{\omega_e^2}{c^2} \frac{\partial \mathbf{B}}{\partial t} - \Omega_e (\mathbf{b} \cdot \nabla) (\nabla \times \mathbf{B}) \\ = \frac{4\pi}{c} \left( -\frac{\partial}{\partial t} \nabla \times \mathbf{J}_s + \Omega_e (\nabla \cdot \mathbf{J}_s) \mathbf{b} - \Omega_e (\mathbf{b} \cdot \nabla) \right. \\ \left. \times \mathbf{J} - \nu_e \nabla_s \times \mathbf{J}_s \right), \end{aligned} \quad (10)$$

where  $\Omega_e = eB_0/m_e c$ ,  $\mathbf{b} = \mathbf{B}_0/|\mathbf{B}_0|$ , and  $\omega_e^2 = 4\pi n_0 e^2/m_e$ . This is the key equation of the paper. Before proceeding with its

solution, it is instructive to examine the evolution of the electric field  $\mathbf{E}(\mathbf{r}, t)$ , for an inertialess ( $m_e=0$ ) and collisionless ( $\nu_e=0$ ) plasma. From Eqs. (7)–(9) we find

$$\frac{\partial \mathbf{E}}{\partial t} - \frac{c^2 \Omega_e}{\omega_e^2} \nabla^2 \mathbf{E} \times \mathbf{b} = \frac{4\pi \Omega_e}{\omega_e^2} \mathbf{b} \times \frac{\partial \mathbf{J}_s}{\partial t}. \quad (11)$$

$$\mathbf{D}(\mathbf{k}, \omega) = i \frac{4\pi}{c} \begin{pmatrix} -ik^2 \omega + i \frac{\omega_e^2}{c^2} \omega + k^2 \nu_e & -k_z^2 \Omega_e & k_y k_z \Omega_e \\ k_e^2 \Omega_e & -ik^2 \omega - i \frac{\omega_e^2}{c^2} \omega - k^2 \nu_e & -k_x k_z \Omega_e \\ -k_y k_z \Omega_e & k_x k_z \Omega_e & -ik^2 \omega - i \frac{\omega_e^2}{c^2} \omega - k^2 \nu_e \end{pmatrix}, \quad (13)$$

and  $\mathbf{J}_{\text{ext}}(\mathbf{k}, \omega)$  is the transform of the external source and is given by

$$\mathbf{J}_{\text{ext}}(\mathbf{k}, \omega) = \frac{4\pi}{c} [\omega \mathbf{k} \times \mathbf{J}_s + i \Omega_e (\mathbf{k} \cdot \mathbf{J}_s) \hat{z} - ik_z \Omega_e \mathbf{J}_s - i \nu_e \mathbf{k} \times \mathbf{J}_s]. \quad (14)$$

The dispersion relation is

$$\mathbf{D}(\mathbf{k}, \omega) = 0. \quad (15)$$

From Eqs. (13) and (15) we find

$$\omega = \frac{kk_z \Omega_e}{k^2 + \omega_e^2/c^2} \left( 1 - i \frac{k \nu_e}{k_z \Omega_e} \right), \quad (16)$$

which represents the propagation mode at low frequencies. For quasiparallel propagation,  $k_z \approx k$ , we recover Eq. (6) corrected for electron inertia and with  $\nu_e/\Omega_e$  corresponding to  $\nu_e/\Omega_e [1 + (\nu_i/\nu_e)(\Omega_e/\Omega_i)]$ , we have

$$\omega = \frac{\Omega_e}{1 + \omega_e^2/k^2 c^2} \left( 1 - i \frac{\nu_e}{\Omega_e} \right). \quad (17)$$

In the following sections, Eq. (10) and its transform will be solved first for a two-dimensional current source (current sheet), given by

$$\mathbf{J}_s(x, z, t) = \begin{cases} \mathbf{e}_x J_0 \delta(z) (1 - e^{-t/\tau}), & |x| < L, \\ 0, & |x| > L, \end{cases} \quad (18)$$

and then for a three-dimensional source,

$$\mathbf{J}_s(x, y, z, t) = \begin{cases} \mathbf{e}_x J_0 \delta(z) \delta(y) (1 - e^{-t/\tau}) u(t), & |x| < L, \\ 0, & |x| > L, \end{cases} \quad (19)$$

where  $u(t)$  is a step function, and  $\tau$  is the rise time of the source.

#### IV. COMPUTATIONAL RESULTS

We now present the results obtained by numerically solving Eq. (10) for the sources given by Eqs. (18) and (19).

We solve Eq. (10) by using a spatial Fourier and temporal Laplace transform (the Appendix). This yields

$$\mathbf{D}(\mathbf{k}, \omega) \cdot \mathbf{B}(\mathbf{k}, \omega) = \mathbf{J}_{\text{ext}}(\mathbf{k}, \omega), \quad (12)$$

where  $\mathbf{D}(\mathbf{k}, \omega)$  is the dielectric tensor of magnetized plasma,

#### A. Response to a current sheet: Collisionless case

Figures 2–6 show the results for the case  $\nu_e=0$ ,  $\omega_e/\Omega_e=1$ ,  $\tau=45\Omega_e^{-1}$ , and length  $L=42c/\omega_e$  for the source given by Eq. (18). The results refer to a current source with  $J_0=1$  mA/m. Figures 2 and 3 show the temporal evolution of the magnetic field  $\mathbf{B}(\mathbf{r}, t)$  as it propagates away from the source.

A pulse induced by the current propagates away on both sides of the source. It is generated during the switch-on and is characterized by strong dispersion with the perturbations with shorter wavelengths running ahead of those with longer wavelengths, as shown in Figs. 2(b) and 2(c). The wave packet exhibits characteristics of the whistler wave and propagates with a group velocity  $c/3$ . Since the group velocity of the parallel propagating whistler is  $V_g = 2c \sqrt{\omega \Omega_e / \omega_e^2}$ , this observed group velocity ( $c/3$ ) corresponds to a frequency  $\omega = \Omega_e/36$ , comparable to the switch-on time  $\tau = 45\Omega_e^{-1}$ . The wave numbers in the wave packets are in the range,  $k \approx 5 - 6 \omega_e/c$ . The identification of the precursor waves as whistlers is clear from the wave polarization (Fig. 3), which shows that the  $B_x$  and  $B_y$  fields in the  $x=0$  plane are  $90^\circ$  out of phase, as expected for these right-hand polarized waves.

The dispersion curve  $\omega$  vs  $k_z$  obtained by computing wavelengths at different frequencies, is displayed in Fig. 4. The computed points fall on the theoretical dispersion curve for whistlers,<sup>13</sup> shown as a solid line in Fig. 4. When the source is turned off, the wave packets disconnect from the source and propagate as isolated wave packets (Fig. 5). This is quite different from the behavior during the switch-on (Fig. 3), during which the radiation field is connected to the source. By turning on and off the cross-field current source, we can generate isolated low-frequency wave packets propagating away on both sides of the current source.

Of particular significance is the identification of the currents induced in the plasma and of the current closure path. This aspect has not been emphasized in the previous studies. The current carried by the excited waves at  $t = 300\Omega_e^{-1}$  is shown in Fig. 6. The initial source current with  $L = 75c/\omega_e$  is

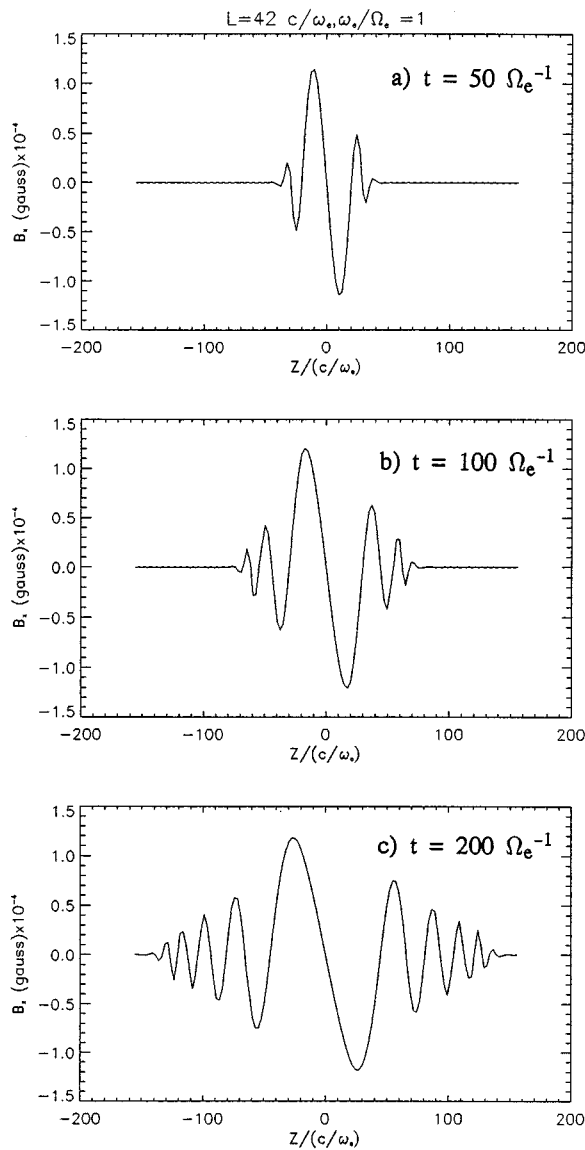


FIG. 2. The amplitudes of the magnetic field component  $B_x$  as a function of  $z$  along the external magnetic field line in the  $x=0$  plane at different times: (a)  $50\Omega_e^{-1}$ , (b)  $100\Omega_e^{-1}$ , and (c)  $200\Omega_e^{-1}$ . The pulse propagates at the group velocity of whistler waves.

shown with a large arrow in the middle, while the plasma currents are proportional to the lengths of the arrows. The complete current path consists of (1) the outgoing portion of the closure current, as represented by the  $J_z$  flowing from the top of the current source outward along the magnetic field connecting the top; (2) the crossover portion of the closure current, as represented by the  $J_x$  flowing across the field and the midplane; and (3) the return portion of the closure current, as represented by the  $J_z$  flowing along the magnetic field toward the bottom of the current source, thus completing the circuit. The two current loops expand along the  $z$  direction, preceded by whistler radiation. The expanding loop has a whistler structure and the front expands in time as

$$Z(t) \approx \frac{c}{\omega_e} \sqrt{\Omega_e t}. \quad (20)$$

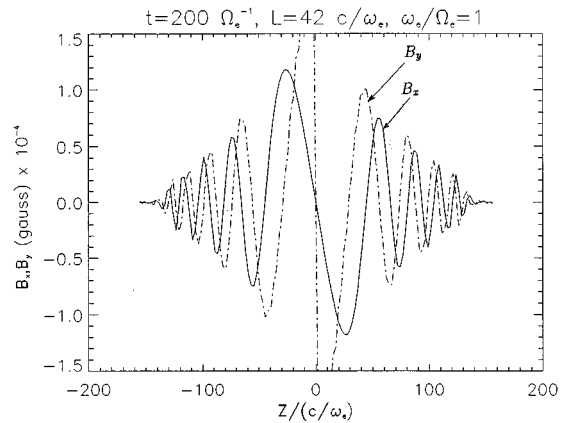


FIG. 3. The magnetic field components  $B_x$  and  $B_y$ , which are  $90^\circ$  out of phase in  $z$ . The excited waves propagate as right-hand circularly polarized waves along the background magnetic field.

The current closure region expands along the external magnetic field with the whistler, the group velocity, and is consistent with the time scale given by Eq. (20). However, the process is weakly dissipative.

We have performed a comprehensive study of the scaling of the field aligned length of the current loop as a function of the plasma parameters, and the results are shown in Fig. 7. The current front moves with the whistler group velocity, which is frequency dependent, and the typical group velocity is computed using a fixed frequency,  $\omega = \Omega_e/170$ . The size of the current closure region is defined by the location of the current reversal away from the source. For example, in Fig. 6, the closure current reverses direction at  $z \approx 45c/\omega_e$ , defining the boundary of the region. The size of the loop  $r$  at a time  $\Omega_e t = 200$  as a function of the electron plasma frequency is shown in Fig. 7(a), and it scales as  $\omega_e^{-1.1}$ . The current closure size at time  $\omega_e t = 200$ , but with  $\omega_e$  constant and  $\Omega_e$  varying, is shown in Fig. 7(b) and the scaling is  $r \sim \Omega_e^{0.64}$ . Finally, Fig. 7(c) shows the closure range as a function of time for the case  $\omega_e/\Omega_e = 1$ , giving a  $t^{0.6}$  scaling.

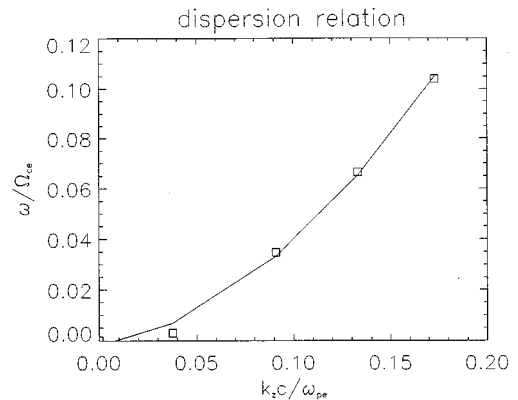


FIG. 4. The normalized dispersion relation, obtained numerically from the wavelengths corresponding to different frequencies (squares) and that given by  $\omega = \Omega_e / (1 + \omega_e^2/k^2 c^2)$  for the given plasma parameter  $\omega_e/\Omega_e = 1$  (solid line). Both polarization and dispersion measurements show that the current perturbations excite whistlers.

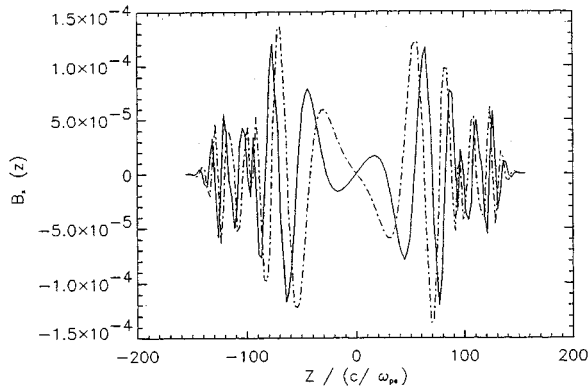


FIG. 5. The magnetic field components  $B_x$  (solid line) and  $B_y$  (dotted line) fields at  $t=200\Omega_e^{-1}$ . The current pulse is turned on at  $t=0$  and turned off at  $t=50\Omega_e^{-1}$ . The plasma parameters are the same as in Fig. 3.

ing. These results confirm the validity of Eq. (20) in describing the loop expansion.

The above results show that the current closure is accomplished at early times. Besides the two field aligned currents, the current closure is accomplished by an electron cross-field Hall current and the closure region expands with the whistler group velocity. The electron Hall current is driven by an electric field  $E_y$ , whose temporal evolution in the  $x$ - $z$  plane is shown in Fig. 8. Notice that the plasma response remains well confined in the transverse direction to a size comparable to  $2L$ , while propagating along  $B$ . We should remark that this transverse confinement was observed in another set of runs (not shown here), with  $L=84c/\omega_e$  and  $168c/\omega_e$ .<sup>14</sup> The cross-field currents at the switch-off showed that current closure pattern is approximately the same as in the switch-on case with the current directions reversed.

An interesting effect related to long time propagation following the switch-off of the source current for the collisionless case can be seen in Fig. 9. It shows contours of the electric field at  $t=2000\Omega_e^{-1}$ , for a source with  $\tau=100\Omega_e^{-1}$ , which is turned off at  $100\Omega_e^{-1}$ . It can be seen that the two

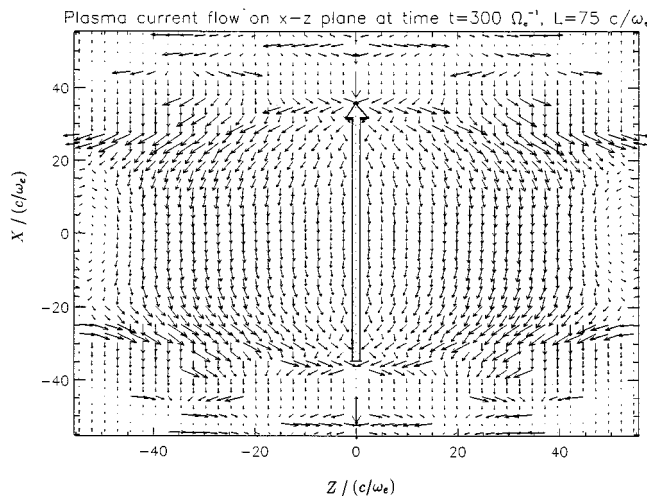


FIG. 6. The plasma current flow in the  $x$ - $z$  plane at time  $t=300\Omega_e^{-1}$ , with  $\Omega_e/\omega_e=1$  and  $\tau=45\Omega_e^{-1}$ . The current source size is  $L=75c/\omega_e$  and the initial current is shown (not to scale) in the middle for comparison.

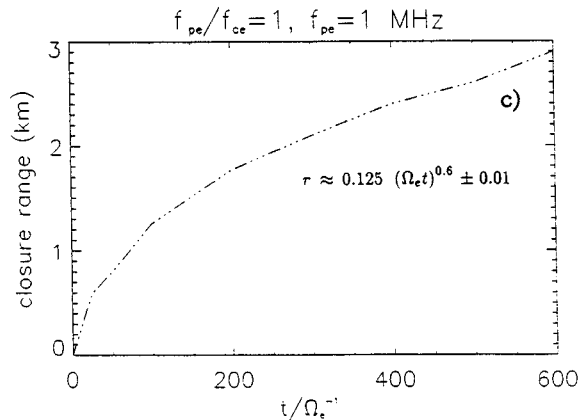
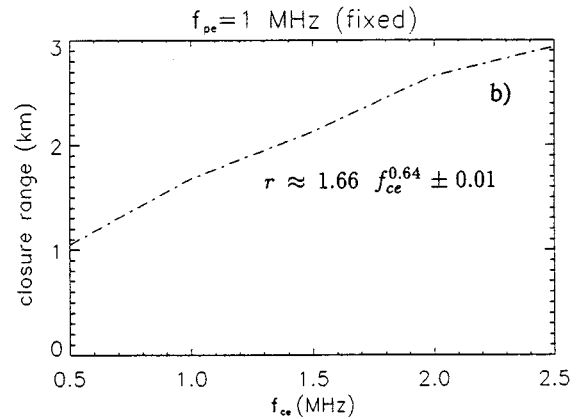
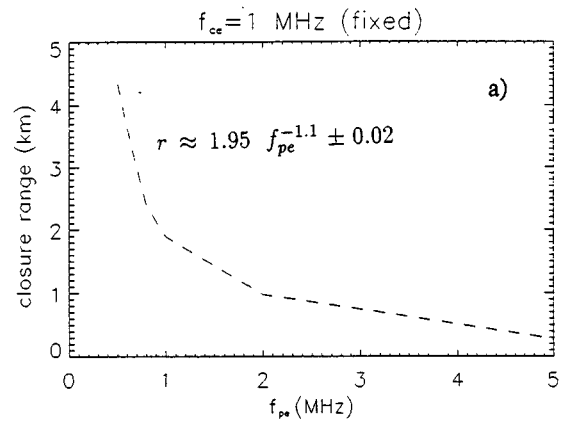


FIG. 7. The scaling of the current closure, (a) closure range as a function of plasma frequency for fixed  $f_{ce}=1$  MHz, (b) closure range as a function of cyclotron frequency for fixed  $f_{pe}=1$  MHz, and (c) closure range as a function of time for  $f_{pe}/f_{ce}=1$ , and  $f_{ce}=1$  MHz.

wave packets disconnect and propagate uncoupled with the characteristic “Story” structure over a  $19^\circ$  angle.<sup>13</sup>

The previous results were constrained to relatively short values of  $\tau$ . On the basis of the physics we expect similar behavior for longer time scales. To confirm this we performed a set of runs with  $\tau=10^4\Omega_e^{-1}$ , the other parameters being  $\omega_e/\Omega_e=2$ , and  $L=84c/\omega_e$  and  $1600c/\omega_e$ . A summary of the results for the evolution of  $B_y$  is shown in Fig. 10 in a different format. The helicon wave packet is highly dispersive, exhibiting characteristics similar to the whistler wave discussed previously. The current closure structure is similar to the one shown in Fig. 6. It should be noted that in the

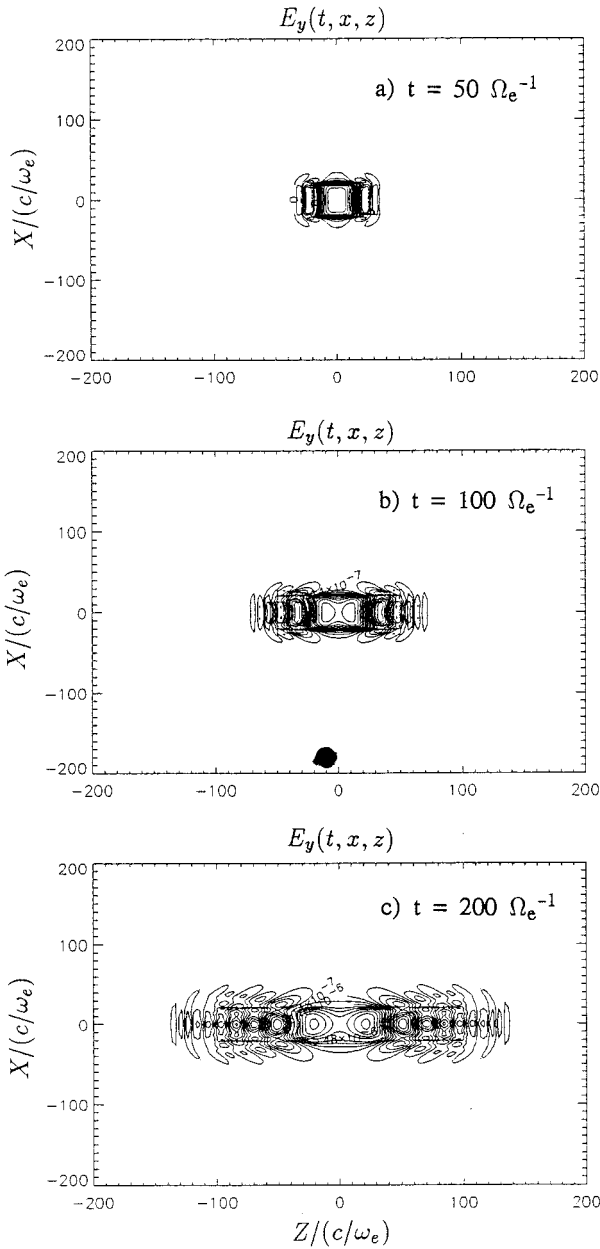


FIG. 8. The contours of  $E_y$  at different times after applying a current pulse across  $B_0$ : (a)  $50\Omega_e^{-1}$ , (b)  $100\Omega_e^{-1}$ , and (c)  $200\Omega_e^{-1}$ .

absence of ion dynamics, these results do not represent the complete physical picture. However, the long time effects of dispersion and dissipation on the propagating wave packets is shown by these results.

In concluding, we note that the observed field and current structures can be understood qualitatively with the following simple physical model. The time-varying current drives an inductive electric field  $E_x = -\partial A_x/\partial t$  that is antiparallel to it when  $\partial I/\partial t > 0$  and parallel when  $\partial I/\partial t < 0$ . Since the electrons are strongly magnetized, this electric field generates only a small polarization current. However, the electrons perform an  $\mathbf{E}_x \times \mathbf{B}_0$  drift that gives rise to a space-charge electric field  $\mathbf{E}_y$  perpendicular to the source current. The consequence of this nonuniform space charge separation is twofold: (1) It gives rise to field-aligned currents  $J_{\parallel}$  that

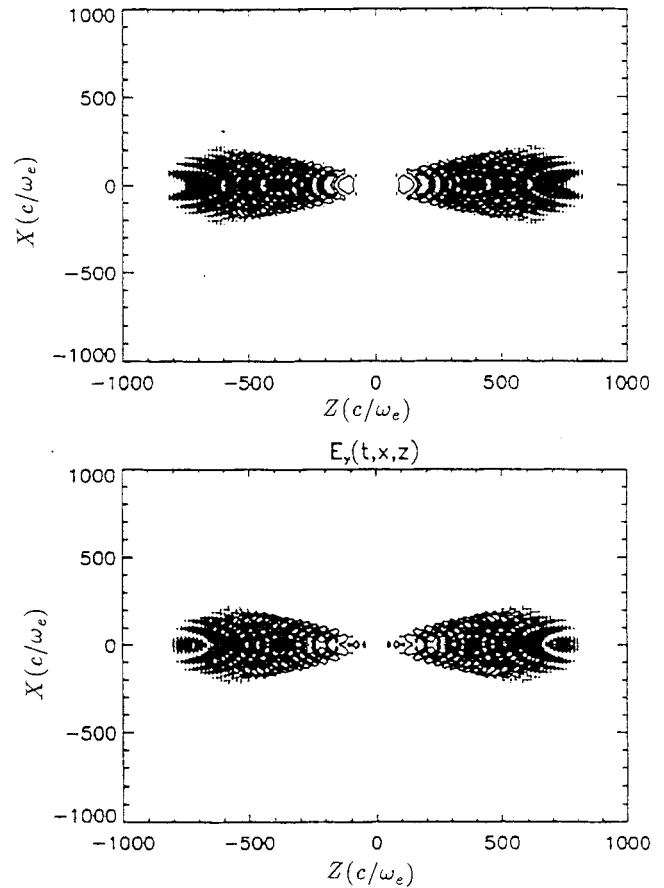


FIG. 9. The contours of  $E_x(x, z)$  and  $E_y(x, z)$  at time  $t = 2000\Omega_e^{-1}$  after applying a current across  $B_0$ . The current pulse is turned on at  $t = 0$  and turned off at  $t = 100\Omega_e^{-1}$ . Note the wavefront spreads in a cone at an angle  $\alpha \approx 20^\circ$  with respect to  $B_0$ .

flows so as to neutralize the excess charges. These field-aligned currents give rise to the observed magnetic field component  $B_x$  shown in Figs. 2 and 3; and (2) the electrons perform an  $\mathbf{E}_y \times \mathbf{B}_0$  drift that gives rise to cross-field currents  $J_x = necE_y/B_0$ , antiparallel to the imposed current. Although this Hall current has the appearance of an induced current, it is not directly driven by the inductive electric field but only indirectly via the space-charge separation.<sup>15</sup> As the current  $J_x$  moves along  $\mathbf{B}_0$  into the plasma, the above processes repeat at the wave front, although with reversed signs: an induced electric field  $-\partial A_x/\partial t$  gives rise to an electron drift  $v_y$ , resulting in a space-charge electric field  $E_y$  and Hall current  $J_x = -\sigma_H E_y$ , with  $\sigma_H = \omega_e^2/4\pi\Omega_e$ . The electron Hall currents, which are not balanced by ion Hall currents, form the cross-field currents.

## B. Collisional and 3-D effects

Although the collective motion of magnetized electrons in a plasma dominates the dynamic response, collisional effects are important. On including collisional effects in the EMHD model, the dispersion relation of whistler/helicon waves in magnetized electron plasma becomes  $\omega = \Omega_e(1 - i\nu_e/\Omega_e)/(1 + \omega_e^2/k^2c^2)$ . The damping rate of the radiation fields due to collisions is controlled by the factor  $\nu_e/\Omega_e$ . We have performed a series of computations with the

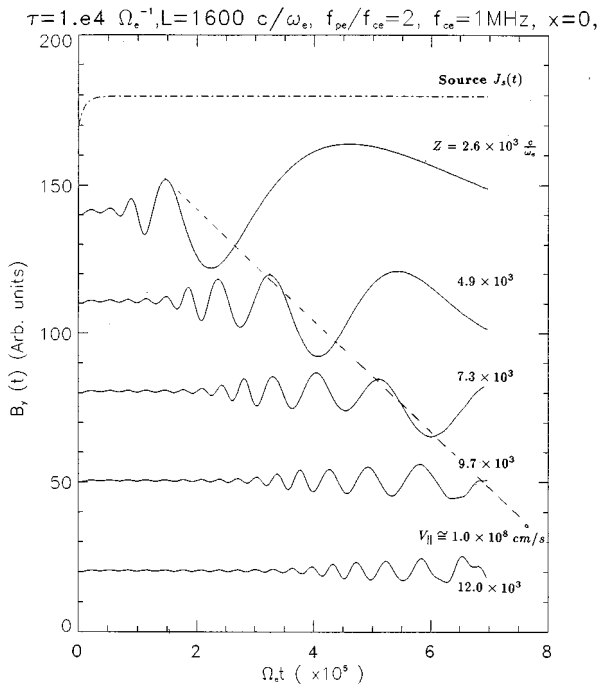


FIG. 10. The time variation of the magnetic field associated with a current switch-on (1 mA, rise time  $\tau=10^4\Omega_e^{-1}$ ) across  $B_0$  through a magnetoplasma. The transient field  $B_y$  at different  $z$  from the source exhibiting wave characteristics along  $B_0$  are shown.

values of the parameters corresponding to those of Figs. 2–6, but with  $\nu_e$  varying between  $(0.001-1)\Omega_e$ . The results for the evolution of  $B_x$  are shown in Fig. 11, at  $t=200\Omega_e^{-1}$ . For  $\nu_e=0.01\Omega_e$ , the wave pattern is similar to the collisionless case [Fig. 2(c)]. When the collision frequency is increased, the waves are gradually damped. For  $\nu_e=0.1\Omega_e$ , the oscillating part of  $B_x$  is damped, while for  $\nu_e=\Omega_e$  the collective mode ceases to exist and the field diffuses into the plasma in a fashion similar to a conventional conductor. The structure of the current loop follows a similar pattern.

For a 3-D time-dependent cross-field current source [Eq. (19)], the current closure pattern is similar to the 2-D case. For the strongly magnetized case, the field-aligned current is shown in Fig. 12 and is closed by electron Hall current (not

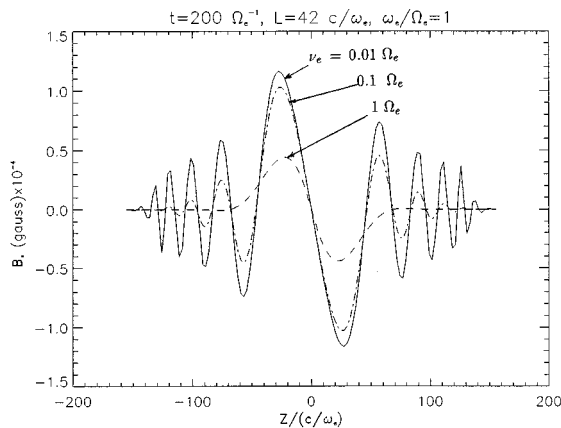


FIG. 11. The effect of collisions on radiation field  $B_x(0,z,t)$  at  $t=200\Omega_e^{-1}$  for collisional frequencies  $\nu_e/\Omega_e=0.01, 0.1$ , and  $1.0$ .

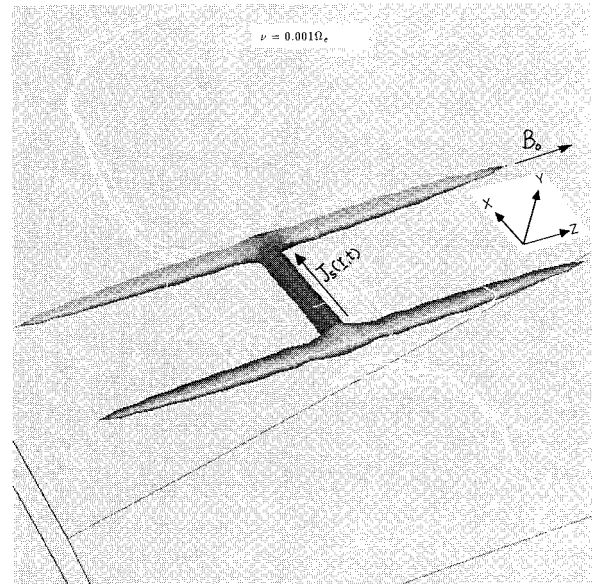


FIG. 12. The isosurface plot of the current density in three dimensions corresponding to a current pulse  $\mathbf{J}_s(\mathbf{r},t)$  imposed across the ambient magnetic field  $B_0$  for a strongly magnetized plasma,  $\nu_e=0.001\Omega_e$ . The outgoing (return) portion of the closure current flowing from the top (bottom) along the ambient magnetic field lines. The cross-field plasma currents are not shown due to their small values in this isosurface plot corresponding to  $J=0.1J_s$ .

shown). In three dimensions the cross-field plasma current is more distributed than in the 2-D case shown in Fig. 6. Consequently the current density is much smaller and does not show in the isosurface plot of the current density, shown in Fig. 12, for  $|J|=0.1J_s$ . The current distribution in the  $x-z$  plane (at  $y=0$ ) for the 3-D distribution (Fig. 12) is shown in Fig. 13. The cross-field current is displayed here, but not shown in Fig. 12. The results obtained using the 3-D time-dependent current source given by Eq. (19) follow the same

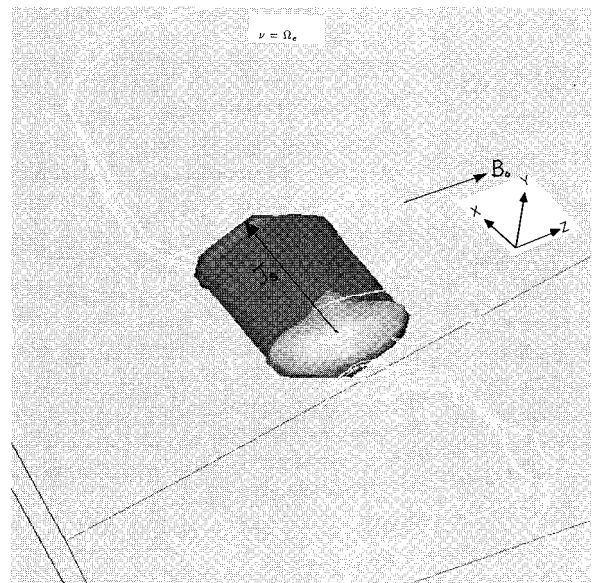


FIG. 13. The three-dimensional plasma current distribution generated by a current pulse  $\mathbf{J}_s(\mathbf{r},t)$  imposed across the ambient magnetic field  $B_0$  for a plasma with  $\nu_e=\Omega_e$ .



general physics of the previous results, although the current path appears more complex. An important result of the 3-D runs is the striking difference of the current path between the weakly collisional ( $\nu_e = 0.001\Omega_e$ ) and the strongly collisional ( $\nu_e = \Omega_e$ ) cases shown in Figs. 12 and 13. Figure 12 shows a strong field-aligned response similar to the two-dimensional case, and the current is again closed by a Hall current (not shown). The three-dimensional features are confined in narrow regions about the field-aligned currents. On the contrary, the strongly collisional case shows a cylindrical distribution of currents about the imposed current, similar to the diffusive response expected when a current pulse is applied on an isotropic conductor. Also, 3-D results show the scale sizes of the current in the  $y$  direction. In Fig. 12 the field-aligned current channels has similar extents in the  $x$  and  $y$  directions. In Fig. 13 the current is distributed in a region that is narrower in the  $y$ -direction.

## V. GENERATION OF ELF/VLF WAVES BY IONOSPHERIC HEATING

A fascinating and important property of the active ionosphere is its potential to act as a frequency transformer that converts HF power injected from the ionospheric heater to coherent VLF/ELF/ULF waves.<sup>5–8</sup> Waves between  $10^{-3}$  Hz and 30 kHz have been generated in the ionosphere by amplitude modulated HF heating in the auroral zones. Ionospheric heating modulates the ambient conductivity, redistributing the ionospheric currents. This acts as an effective ionospheric antenna radiating waves back to the ground or to the magnetosphere at the low modulation frequency. This antenna has often been referred to as the Polar Electrojet Antenna (PEJ). A key issue on the subject is the radiative moment of the PEJ.

Early analysis<sup>7,16</sup> assumed that the radiative moment was a Horizontal Electric Dipole (HED) with moment  $M_E$  given by

$$M_E = E_0 \Delta \sigma L_z L^2, \quad (21)$$

where  $L_z$  is the absorption length of the HF waves in the  $z$  direction and  $L$  is the horizontal dimension of the heated region. In the ionosphere (70–90 km), where the modification takes place,  $\Omega_e > \nu_e$  but  $\Omega_i < \nu_i$ , as a result the EMHD model applies. The results of Sec. IV showed that the plasma responds to a cross-field current, such as the one that creates the assumed HED, by forming a current loop that includes a Hall current in the opposite direction to the applied current. We, therefore, expect that the HED model is incorrect, and should be replaced by a horizontal magnetic dipole (HMD) type source. The objective of this section is to use the EMHD model to determine the type of radiative source and its scaling with frequency and plasma parameters.

### A. Current source by modulated HF heating

In the region of the polar electrojet, a time-varying current source is produced by modulated ionospheric heating. The absorption of a HF wave in the lower ionosphere results in the variation of the electron temperature ( $\Delta T_e$ ) and, to a lesser extent, of the electron density ( $\Delta N_e$ ) at the modulation frequency, and hence to a current modulation. The physics of

the current source generation by modulated ionospheric heating is as follows. At high latitudes the solar wind interaction with the Earth's magnetosphere results in the creation of an electromotive force. Since the magnetic field lines are equipotentials, the high latitude electric field  $\mathbf{E}_0 = E_0 \hat{e}_x$  maps into the lower ionosphere, where collisional processes allow for the generation of cross-field currents. Two types of currents flow across the magnetic field  $\mathbf{B} = B_0 \hat{e}_z$ . The Pedersen current,

$$\mathbf{J}_P = \sigma_P E_0 \hat{e}_x, \quad (22)$$

in the direction of the electric field  $\mathbf{E}_0$ , and the Hall current,

$$\mathbf{J}_H = \sigma_H E_0 \hat{e}_y. \quad (23)$$

In Eqs. (22)–(23),  $\sigma_P$  and  $\sigma_H$  are the Pedersen and Hall conductivities, defined as

$$\sigma_P = \frac{ne^2}{m\Omega_e^2} \frac{\nu_e}{1 + \nu_e^2/\Omega_e^2} \quad \text{and} \quad \sigma_H = \frac{ne^2}{m\Omega_e^2} \frac{\Omega_e}{1 + \nu_e^2/\Omega_e^2}, \quad (24)$$

respectively. Since  $\nu_e$  varies linearly with the electron temperature  $T_e$ , amplitude modulated heating at a low-frequency  $\omega$  induces a modulation on the values of the conductivities through  $\nu_e$ . As is clear from Eq. (24), for heating at altitudes with  $\nu_e \ll \Omega_e$ , the dominant modulation is in the Pedersen conductivity, and this results in a low-frequency modulated cross-field current.

The relevant current density is the height integrated current density  $J_0$  due to the modulation in the temperature. For the case that modification of the Pedersen conductivity dominates, the current generated by modulated HF heating can be written as a series of pulses, with each pulse represented by

$$\mathbf{J}_s(\mathbf{x}, t) = \hat{e}_x S(\mathbf{x}, t) J_0, \quad (25a)$$

$$S(\mathbf{x}, t) = \Theta\left(|x| - \frac{L}{2}\right) \Theta\left(|y| - \frac{\Delta}{2}\right) \delta(z) \times \begin{cases} (1 - e^{-t/\tau}), & t \leq t_0, \\ e^{-(t-t_0)/\tau} - e^{-t/\tau}, & t > t_0, \end{cases} \quad (25b)$$

$$J_0 = j_0 L_z, \quad (25c)$$

where  $\Theta(x)$  is the Heavyside step function,  $L$  and  $\Delta$  are the extensions of the current region in the  $x$  and  $z$  directions, respectively,  $j_0$  is the modified current density, and  $L_z$  the absorption length of the HF power. The values of  $j_0$  and  $L_z$  are given by<sup>10,11</sup>

$$j_0 = \frac{\omega_e^2}{4\pi\Omega_e^2} \frac{\Delta T}{T_0} \nu_e(T_0) E_0, \quad (26a)$$

$$L_z = \frac{c}{\nu_e(T_0)} \frac{\omega_{\text{HF}}^2}{\omega_e^2}, \quad (26b)$$

where  $T_0$  is the ambient temperature,  $\Delta T$  is the modification, and  $\omega_{\text{HF}}$  is the frequency of the HF wave. In applying Eq. (26b), care should be exercised, in that it is valid only if

$$\frac{\omega_{\text{HF}}^2}{\omega_e^2} < \frac{\nu_e}{c} L_N,$$

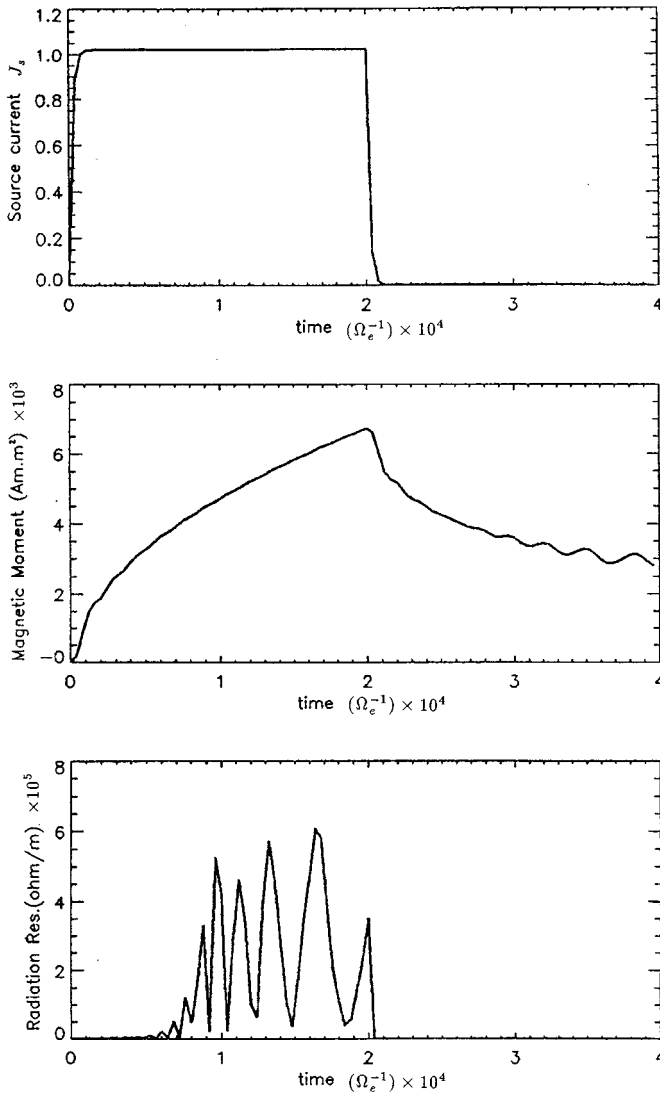


FIG. 14. The current source  $J_s(t)$  generated by modulated HF heating (upper panel), the magnetic moment  $M(t)$  generated by  $J_s(t)$  (middle panel), and the radiation resistance due to  $M(t)$  (lower panel).

where  $L_N$  is the plasma density gradient. From Eq. (26a) and (26b), we find

$$J_0 = \frac{c}{\Omega_e} \left( \frac{\omega_{\text{HF}}^2}{\Omega_e^2} \right) \frac{\Delta T}{T_0} (\Omega_e E_0). \quad (27)$$

### B. Simulations of the PEJ structure

A set of simulations was performed using the code, to determine the expected structure of the PEJ. The parameters were taken as representative of 80–90 km of the ionosphere, with  $f_{ce} = 1$  MHz and  $f_{pe} = 2$  MHz. The simulation box was set in the  $x$ - $z$  plane and covered a region of 120 km in each dimension. A current pulse whose temporal behavior is given by Eq. (25), with  $J_0 = 1$  mA/m,  $L = 20$  km, and  $\Delta = 1$  m, was placed in the middle of the box. The value of the dipole moment was found by the numerical integration of the current moment in the upper half-plane,

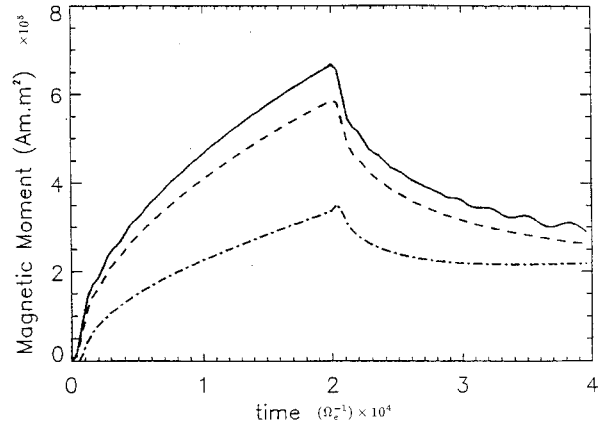


FIG. 15. The integrated magnetic moment as a function of time for different collision frequencies:  $\nu_e = 0.01\Omega_e$  (solid line),  $\nu_e = 0.1\Omega_e$  (dashed line), and  $\nu_e = 0.5\Omega_e$  (dot-dashed line). The current pulse is turned on at  $t = 0$  and turned off at  $t = 2 \times 10^4 \Omega_e^{-1}$ .

$$\mathbf{M} = \frac{1}{2c} \int_{-L/2}^{L/2} dx \int_{-\Delta/2}^{\Delta/2} dy \int_0^\infty dz \mathbf{x} \times \mathbf{J}(x, z, t). \quad (28)$$

For the current source shown in the top panel of Fig. 14, the value of

$$m \equiv \frac{My}{\Delta} = \frac{1}{2c} \int_{-L/2}^{L/2} dx \int_0^\infty dz [zJ_x(x, z, t) - xJ_z(x, z, t)], \quad (29)$$

as a function of time is shown in the middle panel of Fig. 14. In this particular case  $t_0 = 2 \times 10^4 \Omega_e^{-1}$ , corresponding to an ELF frequency of 300 Hz, while  $\nu = 0.01\Omega_e$ . After an initial transient the magnetic moment increases as  $\sqrt{t}$  until the current is turned off. The peak value of  $m$  is  $7 \times 10^5$  A m<sup>2</sup>/m, for  $J_0 = 1$  mA/m, and the minimum value is  $3 \times 10^5$  A m<sup>2</sup>/m, corresponding to a total net radiating moment of  $4 \times 10^5$  A m<sup>2</sup>/m. The temporal variation of  $m(t)$  is due to the radiation of whistler waves propagating upward. A radiation resistance can be computed by integrating the Poynting flux across a detector located, e.g., at  $z = 38$  km. The temporal behavior of the radiation resistance  $R(t)$  is shown in the lower panel of Fig. 14. It is expected that PEJ will radiate whistler waves with instantaneous power  $P(t) = R(t)(J_0 \Delta)^2$ . The role of the collisionality in the value of  $m$  is shown in Fig. 15. It can be seen that the radiative value of  $m$  is relatively insensitive to  $\nu_e$  for  $\nu_e \ll \Omega_e$ . However, the PEJ radiation becomes negligible when  $\nu_e/\Omega_e \approx 1$ . We finally note that varying  $t_0$ , which corresponds to varying the ELF frequency, results in a scaling of  $m \sim \sqrt{t_0} \sim 1/\sqrt{f}$ , where  $f$  is the ELF frequency.

### C. Structure and scaling of the PEJ antenna

From the results of Secs. VI A and VI B we can determine the magnetic moment expected of the PEJ antenna and the resultant scaling by using a three layer model, such as shown in Fig. 16. The upper layer has low collisionality ( $\nu_e/\Omega_e \leq 0.5$ ), whereas the lower layer has high collisionality

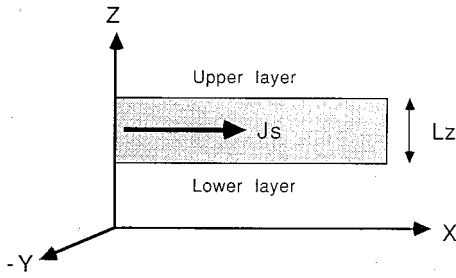


FIG. 16. The three layer model of the magnetic moment.

( $\nu_e/\Omega_e \geq 0.5$ ), and the current flows in the middle layer with  $0.5 \leq \nu_e/\Omega_e \leq 5.0$ . On the basis of the results presented in Sec. V B,

$$M(t) \approx m_u(t) - m_l(t) \approx m_u(t), \quad (30)$$

where  $m_u(m_l)$  are the values of  $M_y/\Delta$  in the upper and lower layers.

The above analysis shows that the horizontal magnetic dipole moment produced by modulated HF heating can be written in mks units as

$$M_y(f) = 6 \times 10^9 \left( \frac{\Delta}{20 \text{ km}} \right) \left( \frac{L}{20 \text{ km}} \right) \times \left( \frac{f_{\text{HF}}}{1.4 \text{ MHz}} \right)^2 \left( \frac{\Delta T}{T_0} \right) \sqrt{\frac{f_0}{f}} \left( \frac{E_0}{\text{V/m}} \right) \text{A m}^2, \quad (31)$$

where  $f_0 = 300$  Hz. In Eq. (30), we note that  $M_y$  scales as  $1/\sqrt{f}$ , and the corresponding power as  $1/f$ . Such behavior is clearly seen in the near-field results ( $f \leq 1$  Hz) of the Tromsø experiments.<sup>17</sup> Similar behavior was observed in the transition from the near- to the far field for frequencies 78 and 154 Hz during high power active stimulation (HIPAS) experiments. Furthermore, during the HIPAS experiments with  $\Delta \sim L \sim 20$  km,  $f_{\text{HF}} \approx 2.8$  MHz and  $f = 154$  Hz,  $M_y$  varied between  $3 \times 10^8 - 2 \times 10^9$  A m<sup>2</sup>. This is consistent with Eq. (32) for values of  $E_0$  varying between 10 and 60 mV/m.

## VI. CONCLUSIONS

The dynamic response of a magnetoplasma to an external time-dependent current source is analyzed within the framework of the EMHD equations. It is shown that, besides short time scales, the EMHD model is a good physical model for the D and E regions of the ionosphere, due to the predominance of ion-neutral collisions. Following a transient emission of whistler/helicon waves, a current loop composed of two field-aligned currents and a transverse Hall current, in addition to the source current, is established. All the dynamics are controlled by the electron flow. The currents are parallel to the perturbed components of the magnetic field and all three components are important. The size of the loop scales as  $\sqrt{\Omega_e t / \omega_e^2}$ . Following the termination of the source, the current loop detaches from the source and damps at a rate controlled by collisions. When  $\nu_e > \Omega_e$  the wave motion disappears and the plasma responds as an isotropic conductor. In a homogeneous plasma two symmetric current loops form

on each side of the source. The presence of inhomogeneities breaks the symmetry, so that the magnetic moments of the loops do not cancel each other.

The results of the study have implications<sup>10,11</sup> in the response of electrodynamic tethers, short term perturbations of the magnetopause and the magnetotail by the solar wind, and on the physics of lower ionosphere when perturbed by natural or artificial sources at any frequency range. In this paper we emphasized the application of the theory to the generation of ELF/VLF radiation by modulated HF heating of the ionosphere. It is shown that, contrary to previous claims, the source region has a magnetic moment consistent with a horizontal magnetic dipole. The importance of the inhomogeneity in the vertical profile of the collision frequency is emphasized. The scaling properties and radiation power generated are determined and shown to be consistent with the experimental data.

Before closing, we should comment on some limitations of the model, arising from the neglect of the wave fields in the electron equation of motion [Eq. (8)]. The results found are linear in the strength of the source and obey the principle of superposition. They are valid up to current densities, such that  $B \ll B_0$ . This condition is easily satisfied for most ionospheric applications, since  $B/B_0$  is at most  $10^{-3}$ . A most stringent condition emerges in the very low collisionality regime and is related to the presence of the parallel electric field  $E_z$ . The value of this field can be estimated as

$$E_z = \frac{(\nu + i\omega)}{\omega_e^2} 4\pi j_z. \quad (32)$$

Since  $j_z$  is proportional to the current level at which phenomena associated with runaway electrons and collective modes would become important. Such phenomena could be important in magnetospheric applications and some tether applications, and will be explored in a future paper.

## ACKNOWLEDGMENTS

This research is supported by the National Aeronautics and Space Administration under Contract No. NAS-51101 and the Office of Naval Research under Grant No. ONR-N0014-93-k-2019.

We would like to thank Dr. Mark Mandt for helpful discussions.

## APPENDIX: EMHD MODEL (STATIONARY SOURCE)

Applying Fourier (with respect to  $x, z$ ) and Laplace transforms (with respect to  $t$ ) on Eq. (10), we obtain the radiation fields in  $(\mathbf{k}, \omega)$  space ( $s = i\omega$ ), as discussed in Sec. III,

$$E_x(\mathbf{k}, s) = i \frac{4\pi\Omega_e}{c} \frac{J_s}{s} \frac{k_x^2 (1 + \nu_e/s) + \omega_e^2/c^2}{\Delta} k_z, \quad (A1)$$

$$B_y(\mathbf{k}, s) = i \frac{4\pi}{c} J_s \times \frac{k^2(1 + \nu_e/s) + k^2 \Omega_e^2/s^2 + (\omega_e^2/c^2)(1 + \nu_e/s)}{\Delta} k_z, \quad (\text{A2})$$

$$B_z(\mathbf{k}, s) = -i \frac{4\pi \Omega_e J_s}{c s} \frac{k_x^2(1 + \nu_e/s) + \omega_e^2/c^2}{\Delta} k_x, \quad (\text{A3})$$

where  $\Delta = [k^2(1 + \nu_e/s) + \omega_e^2/c^2]^2 + (k_x k \Omega_e/s)^2$ . The following current source is introduced into a spatial region that is filled with stationary cold plasma and uniform magnetic field in the  $z$  direction,

$$\mathbf{J}_s(x, z, t) = \begin{cases} \mathbf{e}_x J_0 \delta(z) (1 - e^{-t/\tau}), & |x| < L, \\ 0, & |x| > L. \end{cases} \quad (\text{A4})$$

The Fourier–Laplace transforms of  $J_s(x, z, t)$  is  $J_s(k_x, k_z, s) = 2J_0 \sin k_x L / [k_x s (\tau + 1)]$ , and the inverse Laplace transforms of Eqs. (A1)–(A3) yields

$$B_x(\mathbf{k}, t) = i \frac{8\pi J_0 \Omega_e}{c \tau} \frac{k_z \sin(k_x L)}{k_x (k^2 + \omega_e^2/c^2)^2} \left[ \left( m_{x1} \tau + \frac{m_{x2}}{A_1} + \frac{m_{x3}}{A_2} \right) - m_{x1} \tau e^{-t/\tau} - \frac{m_{x2}}{A_1} e^{-A_1 t} - \frac{m_{x3}}{A_2} e^{-A_2 t} \right], \quad (\text{A5})$$

$$B_y(\mathbf{k}, t) = i \frac{8\pi J_0}{c \tau} \frac{k_z \sin(k_x L)}{k_x (k^2 + \omega_e^2/c^2)^2} \left[ \left( m_{y1} \tau + \frac{m_{y2}}{A_1} + \frac{m_{y3}}{A_2} \right) - m_{y1} \tau e^{-t/\tau} - \frac{m_{y2}}{A_1} e^{-A_1 t} - \frac{m_{y3}}{A_2} e^{-A_2 t} \right] \quad (\text{A6})$$

$$B_z(\mathbf{k}, t) = -k_x/k_z B_x(\mathbf{k}, t). \quad (\text{A7})$$

The triads  $(m_{x1}, m_{x2}, m_{x3})$  and  $(m_{y1}, m_{y2}, m_{y3})$  are the solutions of the following linear equations.

$$\mathbf{T} \cdot \begin{pmatrix} m_{x1} \\ m_{x2} \\ m_{x3} \end{pmatrix} = \begin{pmatrix} 0 \\ k_x^2 + \frac{\omega_e^2}{c^2} \\ k_x^2 \nu_e \end{pmatrix},$$

$$\mathbf{T} \cdot \begin{pmatrix} m_{y1} \\ m_{y2} \\ m_{y3} \end{pmatrix} = \begin{pmatrix} k^2 + \omega_e^2/c^2 \\ \nu_e (2k^2 + \omega_e^2/c^2) \\ k^2 (\nu_e^2 + \Omega_e^2) \end{pmatrix}, \quad (\text{A8})$$

where

$$T = \begin{pmatrix} 1 & 1 & 1 \\ A_1 + A_2 & 1/\tau + A_2 & 1/\tau + A_1 \\ A_1 A_2 & A_2/\tau & A_1/\tau \end{pmatrix}, \quad (\text{A9})$$

and  $A_1 = k(-k\nu_e + ik_z \Omega_e)/(k^2 + \omega_e^2/c^2)$ ,  $A_2 = k(-k\nu - ik_z \Omega_e)/(k^2 + \omega_e^2/c^2)$

We can now transform  $\mathbf{B}(\mathbf{k}, t)$ , given by Eqs. (A5)–(A7), numerically to obtain radiation fields and plasma currents in  $(\mathbf{r}, t)$  space by using two-dimensional inverse FFT techniques.

<sup>1</sup>L. B. Felsen and N. Marcuvitz, *Radiation and Scattering of Waves* (Prentice–Hall, Englewood Cliffs, NJ, 1973).

<sup>2</sup>H. H. Kuehl, *Phys. Fluids* **5**, 1095 (1962).

<sup>3</sup>R. J. Vidmar, F. W. Crawford, and K. J. Harker, *Radio Sci.* **18**, 1337 (1983).

<sup>4</sup>K. C. Budden, *The Propagation of Radio Waves* (Cambridge University Press, Cambridge, 1985).

<sup>5</sup>G. G. Getmantsev, N. A. Zuikov, D. S. Kotik, L. F. Mironenko, N. A. Mityakov, V. O. Rapoport, Yu. A. Sazonov, V. Yu. Trakhtengerts, and V. Ya. Eidman, *JETP Lett.* **20**, 229 (1974).

<sup>6</sup>R. Barr and P. Stubbe, *Radio Sci.* **19**, 1111 (1984).

<sup>7</sup>P. Stubbe and H. Kopka, *J. Geophys. Res.* **82**, 2319 (1977).

<sup>8</sup>K. Papadopoulos, A. S. Sharma, and C. L. Chang, *Comments Plasma Phys. Controlled Fusion* **13**, 1 (1989).

<sup>9</sup>V. L. Ginzburg, *Propagation of Electromagnetic Waves in Plasmas* (Gordon & Breach, New York, 1964).

<sup>10</sup>K. Papadopoulos, H. B. Zhou, and A. S. Sharma, *Comments Plasma Phys. Controlled Fusion* **15**, 321 (1994).

<sup>11</sup>K. Papadopoulos, H. B. Zhou, and C. L. Chang, *Geophys. Res. Lett.* **21**, 1767 (1994).

<sup>12</sup>A. S. Kingsep, K. V. Chukbar, and V. V. Yankov, in *Reviews of Plasma Physics*, edited by M. A. Leontovich (Consultants Bureau, New York, 1990), Vol. 16, p. 243.

<sup>13</sup>R. A. Helliwell, *Whistlers and Related Ionospheric Phenomena* (Stanford University Press, Stanford, 1965).

<sup>14</sup>H. B. Zhou, “Dynamic response of a magnetized plasma to an external source: Application to space and solid state plasmas,” Ph.D. thesis, 1994, University of Maryland, College Park, MD.

<sup>15</sup>R. L. Stenzel, J. M. Urrutia, and C. L. Rousculp, *Phys. Plasmas* **B 2**, 325 (1993).

<sup>16</sup>C. L. Chang, V. Tripathi, K. Papadopoulos, J. Fedder, P. J. Palmadesso, and S. L. Ossakow, in *Effect of the Ionosphere on Radio Systems*, edited by J. M. Godman (U.S. Government Printing Office, Washington, DC, 1981), p. 91.

<sup>17</sup>R. Barr and P. Stubbe, *J. Atmos. Terr. Phys.* **46**, 315 (1984).

<sup>18</sup>C. L. Chang, A. S. Lipatov, A. T. Drobot, K. Papadopoulos, and P. Satyanarayana, *Geophys. Res. Lett.* **21**, 1015 (1994).

<sup>19</sup>D. Kahner, C. Moler, and S. Nash, *Numerical Methods and Software* (Prentice–Hall, Englewood Cliffs, NJ, 1989).